AIAA 81-4225

Instability and Transition in Rotating Disk Flow

Mujeeb R. Malik*
Systems and Applied Science Corporation, Hampton, Va.
Stephen P. Wilkinson†
NASA Langley Research Center, Hampton, Va.
and
Steven A. Orszag‡
Massachusetts Institute of Technology, Cambridge, Mass.

The stability of three-dimensional rotating disk flow is investigated, including the effects of Coriolis forces and streamline curvature. The numerical results show that the critical Reynolds number for establishment of stationary vortex flow is $R_C = 287$. These vortices spiral outward at an angle of about 11.2 deg, and transition to turbulence occurs when their total amplification is about e^{11}. We also report new experimental results on the spatial growth rates of the stationary vortices. It is shown that our analysis gives growth rates that compare much better with the experimental results than do results obtained using the Orr-Sommerfeld equation. The experimental results tend to support the numerical prediction that the number of stationary vortices varies directly with the Reynolds number. Our calculations also indicate the existence of weakly unstable propagating (type II) modes at low Reynolds numbers ($R_C \simeq 49$).

I. Introduction

THE prediction of transition in three-dimensional boundary layers[1-3] is a subject of both fundamental and practical importance in fluid mechanics. Practical interest in the subject centers on the design of laminar flow control (LFC) wings that promise significant improvement in airplane fuel efficiency. At present, the most useful tool for transition prediction in such flows is the so-called e^N method.[4] Hefner and Bushnell[5] and Malik and Orszag[6] show that the exponent N (called the N factor) is of the order 7-11 when transition occurs on LFC swept wings.

The instability mechanism exhibited in the leading-edge region of a swept wing is similar to that found in the boundary layer on a rotating disk, since both have mean cross-flow profiles with inflection points. More details on the similarities between the two flows is given in Ref. 7. The rotating disk flow is amenable to stability analysis in view of von Kármán's exact steady solution[8] of the Navier-Stokes equations free of boundary-layer assumptions.

Using hot-wire techniques, Smith[9] observed that sinusoidal disturbances appear in a rotating disk boundary layer at sufficiently large Reynolds number. About 32 oscillations were observed within a disk rotation period and analysis indicated that the disturbances propagate at an angle of about 14 deg relative to the outward drawn radius (where the direction of disk rotation defines positive angles). Later, in a remarkable study using the china-clay technique, Gregory et al.[10] observed about 30 vortices over the disk spiraling outward at an angle of about 14 deg (that is, their normals make an angle of about 14 deg with the outward drawn radius). These vortices, which appeared stationary relative to the rotating frame of the disk, were first observed at a Reynolds number $R_C \simeq 430$, where R is defined after Eq. (10) below. Transition to turbulence occurred at $R_T \simeq 530$. The stationary vortex flow established due to a rotating disk was later studied by several investigators.[11-13] Among these studies, there exists considerable controversy over the value of the critical Reynolds number which, in our view, can be attributed to the measurement techniques used. There is also some confusion over the number of stationary vortices. Fedorov et al.,[13] using visual (napthalene) and acoustic techniques, observed 27-30 vortices at Reynolds numbers $R \geq 387$. However, at low Reynolds numbers, they observed only 14-16 vortices with normals lying at an angle of about 20 deg.

Stuart[10] analyzed the linear, inviscid stability of rotating disk flow. However, the neglect of viscosity resulted in the prediction of 113-140 vortices over the disk, which is about four times larger than the observed value. Brown[14] extended Stuart's work to the viscous case by applying the Orr-Sommerfeld equation to disk flow. Using the temporal instability theory, Brown found $R_C \simeq 178$, which is much less than the observed value. Recently, Cebeci and Stewartson[3] solved the Orr-Sommerfeld equation for rotating disk profiles using the spatial stability theory and found $R_C \simeq 176$. They also suggested that wave packets propagate in three-dimensional flows in such a way that $d\alpha/d\beta$ is real. Using this condition, Cebeci and Stewartson correlated transition using the e^N method and found the N factor at transition ($R_T = 510$) to be about 20, which is much higher than that found for LFC wings.[5,6] Bushnell[25] argues that a higher N factor may be required for transition in disk flow than on LFC wings because the boundary layer is rotating with the disk while the external disturbances in the surroundings are not. Consequently, there is no direct coupling between the external disturbances and the instability waves in the rotating disk boundary layer.

The Orr-Sommerfeld stability equation neglects the effects of Coriolis forces, streamwise curvature, and nonparallel flow. In Ekman layer flow, Lilly[15] has shown that the Coriolis force has a significant effect on stability at low Reynolds numbers. Lilly showed that the critical Reynolds number for appearance of stationary vortices is higher ($R_C \simeq 115$) when the Coriolis force is included in the analysis than when it is neglected ($R_C \simeq 85$). In addition to the stationary vortices, he showed the existence of another (type II) instability caused by the Coriolis force at much lower Reynolds numbers. Such an instability mechanism was also observed in the Ekman layer experiments of Faller and Kaylor[16] and Tatro and Mollo-Christensen.[17] The Ekman layer and the rotating disk are similar in that both are three-dimensional boundary-layer flows in which rotation plays a

Received Aug. 20, 1980; revision received Feb. 20, 1981.

*Principal Scientist. Member AIAA.

†Aerospace Technologist. Member AIAA.

‡Professor of Applied Mathematics. Member AIAA.

significant role. Lilly's results suggest that the inclusion of the Coriolis force in the stability analysis of rotating disk flow may also lead to a higher critical Reynolds number for stationary vortices, which is in better agreement with observations.

In this paper we present a stability analysis of rotating disk flow in which the effects of Coriolis force and streamline curvature are included. The resulting sixth-order system is solved numerically by a Chebyshev spectral method.[18,19] We also follow the evolution of the disturbance modes using the envelope method[1,6] and calculate the N factor at transition. The work of Kobayashi et al.,[12] which appeared during the final stages of the present study, also includes the effects of the Coriolis force and streamline curvature. We will comment on this work in Sec. VI.

We also report results of an experimental investigation of rotating disk flow in which the growth rates of the boundary-layer disturbances were measured using a hot-wire probe. The experiment showed that the number of stationary vortices increases radially. While only limited experimental results are now available, the present theoretical analysis seems encouraging.

II. Theoretical Analysis

Consider an infinite plane rotating about its axis with angular velocity Ω. We take cylindrical coordinates r^*, θ, z^* with $z^*=0$ being the plane of the disk and assume the fluid to lie in the half-space $z^*>0$. Let $\bar{p}$, $\bar{u}$, $\bar{v}$, $\bar{w}$, denote the steady-state values of pressure and velocity in the r^*, θ, z^* directions, respectively, in the rotating coordinate frame. von Kármán's exact solution[8] of the Navier-Stokes equations for steady laminar rotating disk flow is obtained by setting

$$\bar{u}=r^*\Omega F(z),\quad \bar{v}=r^*\Omega G(z),\quad \bar{w}=\sqrt{\nu\Omega}H(z),\quad \bar{p}=\rho\nu\Omega P(z) \tag{1}$$

where $z=z^*\sqrt{\Omega/\nu}$. The Navier-Stokes equations reduce to the following equations for F, G, H, and P:

$$F^2-(G+1)^2+F'H-F''=0 \tag{2}$$

$$2F(G+1)+G'H-G''=0 \tag{3}$$

$$P'+HH'-H''=0 \tag{4}$$

$$2F+H'=0 \tag{5}$$

where the prime denotes differentiation with respect to z. The boundary conditions are

$$\begin{aligned} &F=0, \quad G=0, \quad H=0 \qquad (z=0)\\ &F=0, \quad G=-1 \qquad (z\to\infty) \end{aligned} \tag{6}$$

Now we study the evolution of infinitesimal small disturbances imposed on the steady flow governed by Eqs. (1-5). Let r_e^* be the radial location near which the analysis is to be made. Using $r_e^*\Omega$ as the reference velocity, $\delta^*=\sqrt{\nu/\Omega}$ as the reference length, and $\rho r_e^{*2}\Omega^2$ as the reference pressure, the instantaneous nondimensional velocities u, v, w and pressure p can be written as

$$u(r,\theta,z,t)=(r/R)F(z)+\tilde{u}(r,\theta,z,t) \tag{7}$$

$$v(r,\theta,z,t)=(r/R)G(z)+\tilde{v}(r,\theta,z,t) \tag{8}$$

$$w(r,\theta,z,t)=(1/R)H(z)+\tilde{w}(r,\theta,z,t) \tag{9}$$

$$p(r,\theta,z,t)=(1/R^2)P(z)+\tilde{p}(r,\theta,z,t) \tag{10}$$

Here the nondimensional radius is $r=r^*\sqrt{\Omega/\nu}$, the Reynolds number is $R=r_e^*\sqrt{\Omega/\nu}$, and r_e^* corresponds to $r=R$.

Substituting Eqs. (7-10) in the Navier-Stokes equations and linearizing with respect to the perturbations gives:

$$\begin{aligned} &\frac{\partial\tilde{u}}{\partial t}+\frac{r}{R}F\frac{\partial\tilde{u}}{\partial r}+\frac{G}{R}\frac{\partial\tilde{u}}{\partial\theta}+\frac{H}{R}\frac{\partial\tilde{u}}{\partial z}+\frac{F}{R}\tilde{u}\\ &-\frac{2}{R}(G+1)\tilde{v}+\frac{r}{R}F'\tilde{w}=-\frac{\partial\tilde{p}}{\partial r}+\frac{1}{R}\left[\frac{\partial^2\tilde{u}}{\partial r^2}\right.\\ &\left.+\frac{1}{r^2}\frac{\partial^2\tilde{u}}{\partial\theta^2}+\frac{\partial^2\tilde{u}}{\partial z^2}+\frac{1}{r}\frac{\partial\tilde{u}}{\partial r}-\frac{2}{r^2}\frac{\partial\tilde{v}}{\partial\theta}-\frac{\tilde{u}}{r^2}\right] \end{aligned} \tag{11}$$

$$\begin{aligned} &\frac{\partial\tilde{v}}{\partial t}+\frac{r}{R}F\frac{\partial\tilde{v}}{\partial r}+\frac{G}{R}\frac{\partial\tilde{v}}{\partial\theta}+\frac{H}{R}\frac{\partial\tilde{v}}{\partial z}+\frac{F}{R}\tilde{v}\\ &+\frac{2}{R}(G+1)\tilde{u}+\frac{r}{R}G'\tilde{w}=-\frac{1}{r}\frac{\partial\tilde{p}}{\partial\theta}+\frac{1}{R}\left[\frac{\partial^2\tilde{v}}{\partial r^2}\right.\\ &\left.+\frac{1}{r^2}\frac{\partial^2\tilde{v}}{\partial\theta^2}+\frac{\partial^2\tilde{v}}{\partial z^2}+\frac{1}{r}\frac{\partial\tilde{v}}{\partial r}+\frac{2}{r^2}\frac{\partial\tilde{u}}{\partial\theta}-\frac{\tilde{v}}{r^2}\right] \end{aligned} \tag{12}$$

$$\begin{aligned} &\frac{\partial\tilde{w}}{\partial t}+\frac{r}{R}F\frac{\partial\tilde{w}}{\partial r}+\frac{G}{R}\frac{\partial\tilde{w}}{\partial\theta}+\frac{H}{R}\frac{\partial\tilde{w}}{\partial z}+\frac{H'}{R}\tilde{w}\\ &=-\frac{\partial\tilde{p}}{\partial z}+\frac{1}{R}\left[\frac{\partial^2\tilde{w}}{\partial r^2}+\frac{1}{r^2}\frac{\partial^2\tilde{w}}{\partial\theta^2}+\frac{\partial^2 w}{\partial z^2}+\frac{1}{r}\frac{\partial\tilde{w}}{\partial r}\right] \end{aligned} \tag{13}$$

$$\frac{\partial\tilde{u}}{\partial r}+\frac{1}{r}\frac{\partial\tilde{v}}{\partial\theta}+\frac{\partial\tilde{w}}{\partial z}+\frac{\tilde{u}}{r}=0 \tag{14}$$

The boundary conditions are that $\tilde{u}$, $\tilde{v}$, and $\tilde{w}$ vanish at $z=0,\infty$.

For $R\gg 1$, the system of Eqs. (11-14) may be consistently approximated by replacing factors of r by R and neglecting terms of order R^{-2} and smaller. The replacement of r by R at this stage of the calculation implies that we neglect some nonparallel flow effects. The neglect of terms of order R^{-2} and smaller has little effect on the results discussed below, as we verified by computations in which they were included.

Replacing factors of r by R in Eqs. (11-14) gives a set of equations that is separable in r, θ, t so that the perturbation quantities may be assumed to have the form

$$(\tilde{u},\tilde{v},\tilde{w},\tilde{p})=(f(z),h(z),\phi(z),\pi(z))\exp[i(\alpha r+\beta R\theta-\omega t)] \tag{15}$$

With this assumption, Eqs. (11-14) become (not yet dropping terms of order R^{-2})

$$\begin{aligned} &i(\alpha F+\beta G-\omega)f+F'\phi+i\alpha\pi=(1/R)[f''-\lambda^2 f-Ff\\ &+2(G+1)h-Hf']+(1/R^2)[i\alpha f-2i\beta h]-(1/R^3)f \end{aligned} \tag{16}$$

$$\begin{aligned} &i(\alpha F+\beta G-\omega)h+G'\phi+i\beta\pi=(1/R)[h''-\lambda^2 h-Fh\\ &-2(G+1)f-Hh']+(1/R^2)[i\alpha h+2i\beta f]-(1/R^3)h \end{aligned} \tag{17}$$

$$\begin{aligned} &i(\alpha F+\beta G-\omega)\phi+\pi'=(1/R)[\phi''-\lambda^2\phi\\ &-H\phi'-H'\phi]+(i/R^2)\alpha\phi \end{aligned} \tag{18}$$

$$[i\alpha+(1/R)]f+i\beta h+\phi'=0 \tag{19}$$

where $\lambda^2=\alpha^2+\beta^2$.

Eliminating π from Eqs. (16-18) by means of Eq. (19) gives, neglecting terms of order R^{-2} and smaller,

$$\begin{aligned} &(1/R)[i(D^2-\lambda^2)(D^2-\bar{\lambda}^2)+R(\alpha F+\beta G-\omega)(D^2-\bar{\lambda}^2)\\ &-R(\alpha F''+\beta G'')-iHD(D^2-\bar{\lambda}^2)-iH'(D^2-\bar{\lambda}^2)\\ &-iFD^2]\phi+(1/R)[2(G+1)D+2G']\eta=0 \end{aligned} \tag{20}$$

$$(1/R)[2(G+1)D-iR(\alpha G'-\beta F')]\phi+(1/R)[i(D^2-\lambda^2)$$
$$+R(\alpha F+\beta G-\omega)-iHD-iF]\eta=0 \quad (21)$$

where $D=\mathrm{d}/\mathrm{d}z$, $\bar{\alpha}=\alpha-i/R$, $\bar{\lambda}^2=\alpha\bar{\alpha}+\beta^2$ and $\eta=\alpha h-\beta f$ is proportional to the z component of the perturbation vorticity. The final result, Eqs. (20) and (21), is a consistent set of stability equations valid to order R^{-1}.

The boundary conditions for the sixth-order system, Eqs. (20) and (21), are

$$\phi(0)=\phi'(0)=\eta(0)=0, \quad \phi(\infty)=\phi'(\infty)=\eta(\infty)=0 \quad (22)$$

Note that if the Coriolis force and streamline curvature effects are neglected, the above system reduces to the fourth-order Orr-Sommerfeld equation

$$[i(D^2-\lambda^2)^2+R(\alpha F+\beta G-\omega)(D^2-\lambda^2)$$
$$-R(\alpha F''+\beta G'')]\phi=0 \quad (23)$$

In Sec. VI, we report numerical results for both the sixth-order system, Eqs. (20) and (21), and the fourth-order equation, Eq. (23), in order to study the effect of the Coriolis force and streamline curvature terms on the stability of flow due to a rotating disk.

III. Numerical Method

We solve the Orr-Sommerfeld equation (23) using the computer code SALLY,[1] which employs a spectral method based on Chebyshev polynomials.[18,19] Here we extend the method to solve the sixth-order system, Eqs. (20-22).

The boundary-layer coordinate z, $0\le z<\infty$ is mapped into the finite interval $-1\le\xi<1$ by the algebraic mapping

$$\xi=2[z/(z+L)]-1 \quad (24)$$

where L is a scale parameter chosen to optimize the distribution of points in ξ. Then $\phi(z)$ and $\eta(z)$ are approximated as the finite Chebyshev polynomial series

$$\phi(z)=\sum_{n=0}^{M} a_n T_n(\xi) \quad (25)$$

$$\eta(z)=\sum_{n=0}^{M} b_n T_n(\xi) \quad (26)$$

Substituting Eqs. (25) and (26) in Eqs. (20-22) and collocating Ref. 19 at the discrete points $\xi_j=\cos\pi j/M$ $(0\le j\le M)$ gives the algebraic eigenvalue problem

$$A\begin{Bmatrix} a_n \\ b_n \end{Bmatrix}=\omega B\begin{Bmatrix} a_n \\ b_n \end{Bmatrix} \quad (27)$$

where A and B are $2(M+1)\times 2(M+1)$ matrices. The eigenvalue problem, Eq. (27), is solved globally (if a guess for an eigenvalue is not available) by a generalized QR algorithm or locally (if a good guess is available) by inverse Rayleigh iteration.[20] The resulting scheme is very efficient and accurate. In the present calculations, the optimum value of the scaling parameter L was found to be about 1.8. In most of the calculations reported below, $M=34$, so 35 Chebyshev polynomials were used.

The accuracy of the method was tested in several ways. First, the number of retained polynomials, $M+1$ was varied to check the accuracy of the eigenvalues and eigenfunctions. Then, calculations were made for the stability of Ekman flow. Comparisons were made with the results obtained by Lilly[15] for $R=65$, 110, 150, 300, and 500 with good agreement.

For rotating disk flow, the global method gives only one unstable eigenvalue $[\mathrm{Im}(\omega)>0]$ for $R\gtrsim 150$ that is insensitive to M. However, spurious unstable modes appear for lower R, which are discarded as unphysical because they are very sensitive to M.

IV. Transition Prediction Using the e^N Method

In three-dimensional flow, the dispersion relation is given by the complex relation

$$\omega=\omega(\alpha,\beta) \quad (28)$$

where α, β, and ω are, in general, complex. Therefore, there are four arbitrary real parameters among α, β, and ω. There are several ways[6] to remove this arbitrariness. In the present study we employ the envelope method.[1] Here the four conditions are obtained by using temporal stability theory [in which $\mathrm{Im}(\alpha)=\mathrm{Im}(\beta)=0$] and by maximizing $\mathrm{Im}(\omega)$ with respect to α, β at fixed $\mathrm{Re}(\omega)$. The N factor is then given by

$$N=\int_{s_C}^{s_T}\frac{\mathrm{Im}(\omega)}{|\mathrm{Re}(v_g)|}\mathrm{d}s \quad (29)$$

where $v_g=(\omega_\alpha,\omega_\beta)$ is the (complex) group velocity and s is the arc length along the curve whose tangent is the real part of the group velocity. Noting that

$$\mathrm{d}s=\frac{\mathrm{d}R}{\mathrm{Re}(\omega_\alpha)}\sqrt{(\mathrm{Re}(\omega_\alpha))^2+(\mathrm{Re}(\omega_\beta))^2}=\frac{\mathrm{d}R}{\mathrm{Re}(\omega_\alpha)}|\mathrm{Re}(v_g)|$$

Eq. (29) can be written as

$$N=\int_{R_C}^{R_T}\frac{\mathrm{Im}(\omega)}{\mathrm{Re}(\omega_\alpha)}\mathrm{d}R \quad (30)$$

where the subscripts C and T indicate critical (linearly unstable) and onset of transition, respectively.

V. Experimental Study

An experimental program was established to quantitatively study the flat rotating disk flow with particular attention given to measurement of the growth of boundary-layer disturbances as a function of Reynolds number.

Rotating Disk Apparatus

The experimental apparatus consisted of a 457-mm-diam plexiglass disk which was mounted on a horizontal shaft. The drive shaft was inserted between two premounted, self-aligning ball bearings and was driven by a 1/4 hp, 1725 rpm ac motor through a 2:1 belt and pulley speed reduction system. Static measurements with a dial indicator showed the disk to have a ± 0.008 mm maximum deviation from a flat plane with four peaks and valleys per revolution.

The assembly was housed in a 1.8 m cubical box with an open front. The radial flow at the disk periphery was ducted behind the disk by placing a 1.8 m square cover several boundary-layer thicknesses in front of the disk, with the test surface exposed by a large hole of slightly smaller diameter than the disk. A single constant temperature, linearized hot-wire anemometer was used to measure the fluctuating circumferential velocity component, $\tilde{v}$. The wire was placed parallel to the disk surface with the wire axis along a radius. The wire was fixed in space while the disk boundary layer rotated past it. The hot-wire signal was bandpass filtered in the range $250<f<600$ Hz.

Broadband vibration of the disk in the axial direction was noted with a spectral peak at 375 Hz and a peak amplitude of 0.35×10^{-6} mm. Due to the large velocity gradient in the boundary layer, velocity fluctuations were not distinguishable

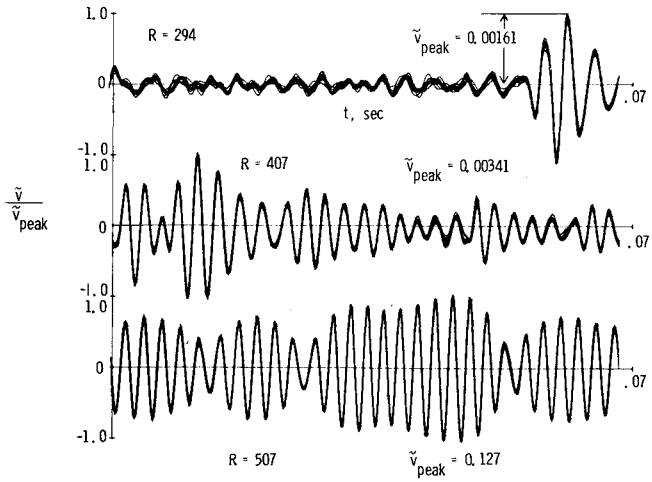

Fig. 1 Peak normalized fluctuating tangential velocity at $G = -0.5$.

from modulation of the hot-wire output by the disk vibration for $R<219$. For R as high as 394, the influence of the vibration was still slightly noticeable.

All measurements were made in room air at a constant unit Reynolds number of $\sqrt{\Omega/\nu} = 2465/\text{m}$ and a constant boundary-layer height corresponding to $G = -0.5$.

All of the data in Fig. 3 show exponential growth for $R>400$. For $R<400$, these data are seen to deviate significantly from the exponential growth rate. The reason for this behavior is most likely the contamination of the data in this very low fluctuation amplitude region by disk vibration.

The disk vibration problem also eliminated the possibility of rigorously determining the experimental critical Reynolds number for the stationary disturbances. These disturbances were first observed on the entire disk in our experiment at $R = 294$ (see Fig. 1). It is, therefore, reasonable to say that the critical Reynolds number for stationary disturbances is somewhat less than 294.

Transition to turbulence as evidenced by the first formation of locally turbulent regions on the disk was observed to occur in the range $513<R<526$. The maximum Reynolds number 538 for this experiment precluded attainment of a fully turbulent flow.

Experimental Results

Instantaneous circumferential velocity fluctuations were digitally recorded for 36 values of R in the range $125<R<538$ at a constant boundary-layer height of $z = 0.93$ ($G = -0.5$). Three sets of such data (peak normalized) are shown in Fig. 1. Each plot is an overlay of 12 successive rotations of the disk. This technique clearly shows that the fluctuations were stationary with respect to the disk. The plot for $R = 294$ was the first for which the stationary disturbance vortices were observed on the entire disk. These vortices were noted to be extremely persistent; that is, the pattern could be intentionally destroyed by imposing a large random air disturbance on the disk flow and the stationary pattern would re-establish itself when the large disturbance damped out. There was also no success in altering the number of stationary vortices by beaming sound at the disk of various sinusoidal frequencies and amplitudes. The amplitude modulation exhibited in Fig. 1 has not been fully explained, but it may be a hot-wire response to relative motion between the hot wire and disk due to the deviation of the disk from true flatness.

Another notable feature of the plots in Fig. 1 is the variation in the number of vortices per revolution from 20-22 at $R = 294$ to 28 at $R = 507$. The increase in the number of vortices is apparently due to a bifurcation phenomenon of the vortices with increasing R. This is an important new finding and we will discuss it at some length in the next section.

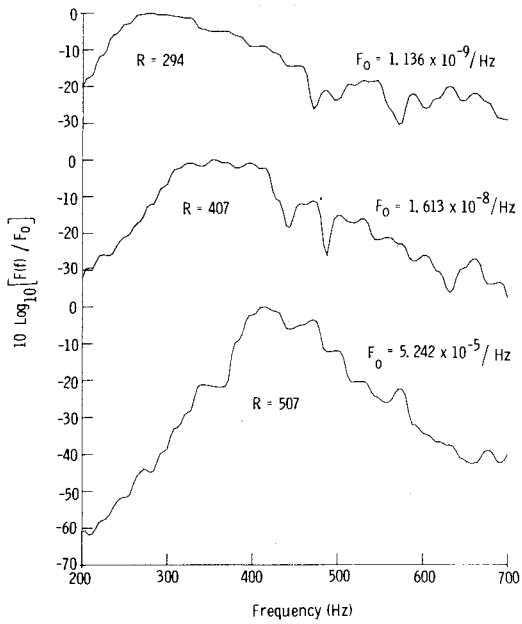

Fig. 2 Spectra of stationary disturbances at $G = -0.5$.

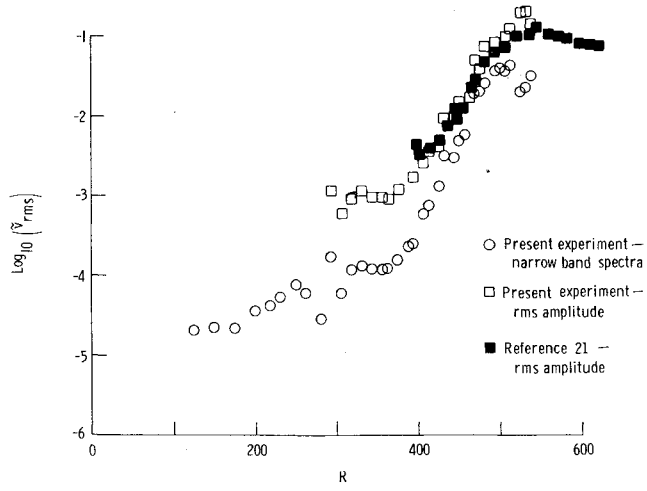

Fig. 3 rms fluctuating tangential velocity at $G = -0.5$.

The normalized rms spectra of the signals shown in Fig. 1 are presented in Fig. 2. $F(f)$ is defined by the relation

$$\overline{\tilde{v}^2} = \int_{f_1}^{f_2} F(f)\,df$$

where $\overline{\tilde{v}^2}$ is the mean square fluctuation in the frequency range $f_1<f<f_2$. The movement of the spectral peak toward higher frequencies is due to the increasing number of vortices.

The amplitude modulation of the signals noted in connection with Fig. 1 caused difficulty in estimating the growth rate of the vortices. Two approximate methods were used. One method was to determine the maximum relative fluctuation amplitude ($\tilde{v}_{max}$) from the digitized data and to calculate its rms value assuming a sinusoidal fluctuation. These data are shown as the open squares in Fig. 3 and are seen to compare favorably with the results of Kitamura.[21] § Kitamura's growth rate data were taken at $z = 1.3$ and scaled to the boundary-layer location of the present experiment using data also presented in Ref. 21. The magnitude of the correction was less than the scatter in the data. The second method of measuring the growth rate was to integrate the rms

§Growth rate data from Ref. 21 were made avilable by private communication with I. Tani.

Table 1 Experimental critical and transition Reynolds numbers for stationary vortex flow

Investigators	Reynolds number			Method of investigation
	Critical	Transition	Onset of transition	
Smith[9]	460	557	–	Hot-wire probe
Gregory et al.[10]	430	530	–	Visual (China-clay technique)
Cobb and Saunders[24]	447	490	–	Heat transfer from the disk
Gregory and Walker[22]	367	524	505	Acoustical slotted disk
Chin and Litt[23]	412	592	510	Mass transfer coefficient using electrochemical
Fedorov et al.[13]	387	515	–	Visual (napthalene), acoustical
Clarkson et al.[11]	532-621	562-680	–	Visual (dye in water)
Kobayashi et al.[12]	297	566	500 (nonlinear)	Hot-wire probe
Present results	294	–	513-526	Hot-wire probe

fluctuation spectrum (see Fig. 2) over a narrow band (± 10 Hz) centered on a frequency determined by the number of observed stationary vortices and the rate of rotation of the disk. For $R < 294$, where a full stationary pattern was not observed, 21 vortices were arbitrarily assumed. As stated above, data in this region are contaminated by hot-wire modulation caused by axial disk vibration and are, therefore, unreliable. Results are presented as the open circles in Fig. 3. The level of the data is significantly lower than that determined using the first method. This is a result of the integration being made over a narrow frequency band, but the indicated growth rate is seen to be similar.

VI. Results and Discussion

Critical and Transition Reynolds Numbers

Some of the available experimental data for critical and transition Reynolds numbers are given in Table 1. It is apparent that there is considerable variation of the observed critical and transition points. We believe that the variation can be attributed to either the different measurement techniques used in the experiments or to the influence of external disturbances. Using the Orr-Sommerfeld equation, we obtained a critical Reynolds number $R_C \simeq 171$, which is in good agreement with the theoretical results of Brown[14] and Cebeci and Stewartson,[3] but is considerably less than the observed values. The value of the critical Reynolds number for stationary disturbances is significantly improved when the effects of Coriolis forces and streamline curvature are included. Our calculated critical Reynolds number of 287 for disturbances of this kind is in excellent agreement with our experimental results and the value of 297 obtained by Kobayashi et al.[12] using hot-wire techniques. Kobayashi et al.[12] also performed a theoretical analysis in which some of the effects of Coriolis forces and streamline curvature were considered. They calculated a critical Reynolds number of 261.

In order to correlate transition using the stability theory, one has to know the experimental location of the onset of transition. The transition Reynolds numbers usually given for experiments (see Table 1) are the locations where transition is complete. Gregory and Walker[22] showed that for a slotted rotating disk, the transition region is composed of two subregions: 1) a vortex region and 2) an intermediate turbulent region where the intermittency factor γ varies from 0 to 1. Stability theory is only applicable up to the point where the first turbulence burst appears ($\gamma = 0$). Gregory and Walker obtained $R = 505$ and 524 for $\gamma = 0$ and $\gamma = 1$, respectively.

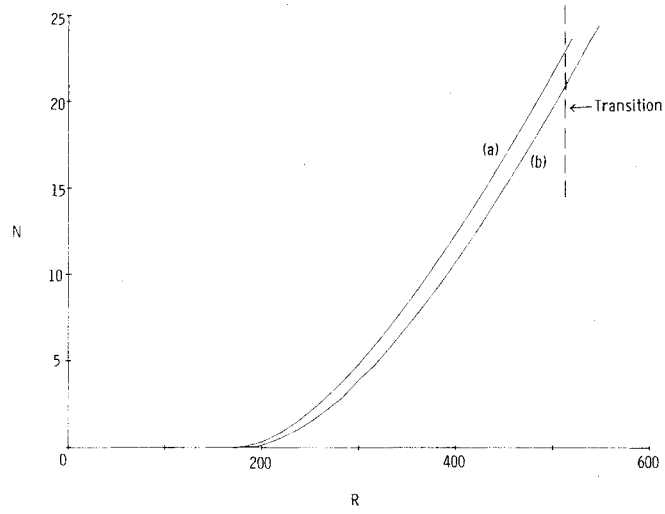

Fig. 4 Integrated growth factor using Orr-Sommerfeld equation: a) present calculations; b) Cebeci and Stewartson.[3]

Chin and Litt,[23] using an electrochemical technique, observed that the transition was complete at $R = 592$. They also observed that the vortices start breaking down into turbulence at $R_T = 510$. We believe that this result should be taken as the relevant location for the onset of transition for the purposes of comparison with stability theory. Further evidence that the initiation of transition occurs at $R_T \simeq 510$ is provided by Kobayashi et al.,[12] who observe that the disturbances are nonlinear at $R = 500$. Usually in boundary-layer flows the nonlineag region is relatively narrow so the onset of transition soon follows. Further, Federov et al.[13] observed turbulent flow at $R = 515$. In our experiment, turbulent spots first appeared at $R = 513$-526. On the basis of our observations and the evidence provided by other investigators,[12,13,22,23] we take $R_T = 513$ as the location of the onset of transition for the purpose of applying the e^N correlation method.

Growth of Infinitesimal Disturbances

Disturbances of all frequencies may be present in natural transition. We follow the evolution of several different modes, and the one which gives the highest integrated growth factor is used to correlate transition. Stationary disturbances were found to give the highest N factor for rotating disk flow over all positive real frequencies. Disturbances with negative

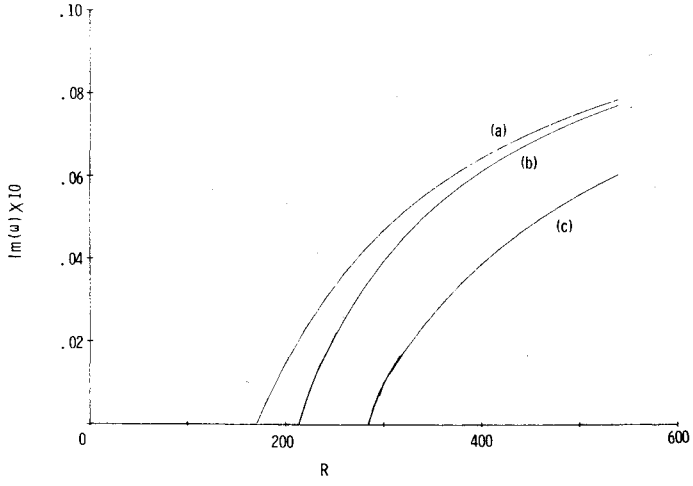

Fig. 5 Temporal growth rates for stationary vortices: a) Orr-Sommerfeld equation; b) Orr-Sommerfeld equation with Coriolis force effects included; c) Orr-Sommerfeld equation with Coriolis force and streamline curvature effects included.

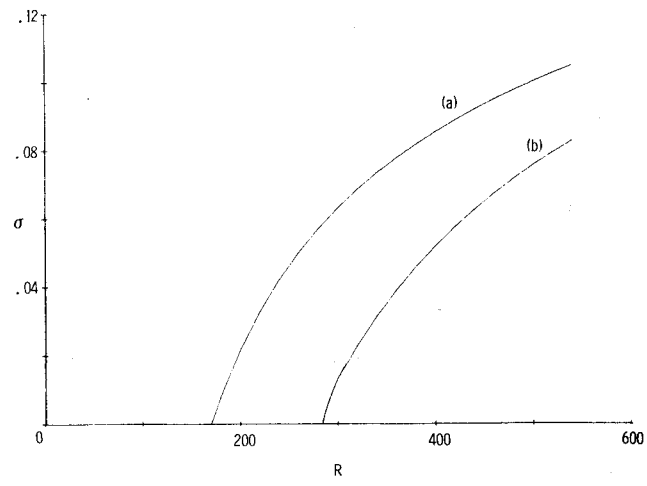

Fig. 6 Spatial growth rates for stationary vortices: a) Orr-Sommerfeld equation; b) present theory.

phase velocities can give slightly higher N factors, but they are of no consequence in the process of transition.

It was shown in Ref. 6 that the envelope method is a reliable tool for transition prediction in three-dimensional flows. First, we report calculations using the Orr-Sommerfeld equation. The resulting N factors are compared with those of Cebeci and Stewartson[3] in Fig. 4. It is evident that their method predicts $N \simeq 20$ at transition ($R = 513$), while the present (envelope) method gives $N \simeq 22$ at transition. Cebeci and Stewartson[3] used spatial stability theory, and in order to remove arbitrariness among the parameters of Eq. (28), they imposed the condition

$$\frac{\partial \alpha_i}{\partial \beta_r} = 0 \tag{31}$$

where $\alpha_i = \mathrm{Im}(\alpha)$, $\beta_r = \mathrm{Re}(\beta)$. In order to simplify their computations, Cebeci and Stewartson assumed that the maximum growth rate at any $R > R_C$ is independent of the growth direction. We believe that had their growth rates been maximized over all possible growth directions, their N factor at transition would be in better agreement with the present predictions using the Orr-Sommerfeld equation.

In Fig. 5 we plot calculated temporal growth rates Im(ω) for stationary vortices. It can be seen that inclusion of streamline curvature and Coriolis forces have a significant stabilizing effect. Calculations with only Coriolis terms (as done by Lilly[15] for Ekman flow) were also made. These results indicate that streamline curvature effects must also be included in order to model properly the physical problem.

Since the instability is spatial in nature, we transform temporal growth rates to spatial growth rates σ using the group velocity transformation

$$\sigma = \mathrm{Im}(\omega)/\mathrm{Re}(\omega_\alpha) \tag{32}$$

The spatial growth rates are plotted in Fig. 6. The effect of streamline curvature and Coriolis forces is found to be very significant.

Integrated growth rate (N factor) results are presented in Fig. 7. The present stability theory gives $N \simeq 10.7$, which is close to the value $N = 9$ for two-dimensional flows and is in the range of values found for swept wings.[6] It is apparent that there is a very significant effect on the predicted transition N factor when the effects of Coriolis forces and streamline curvature are included. The resulting N factors are much lower than those obtained by conventional stability theory where only the Orr-Sommerfeld equation is solved.

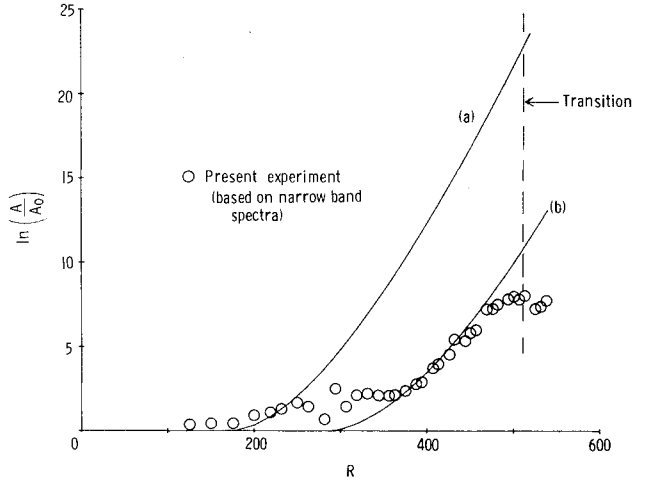

Fig. 7 Integrated growth factor for stationary vortices: a) Orr-Sommerfeld equation; b) present theory.

Also presented in Fig. 7 are experimental results for the N factor. The experimental amplification rate of the stationary vortices was determined by integrating the rms fluctuation spectrum in a narrow band centered on a frequency determined by the observed number of vortices, as described in Sec. V. Due to the problem with disk vibrations indicated earlier, the disturbance amplitude (A_0) at the minimum critical Reynolds number could not be measured with any certainty. It was assumed that $A_0 = 1$ and the resultant data were shifted at constant Reynolds number to match the theoretical growth curve. The data are seen to be in fair agreement with the present theory over the range $400 < R < 500$. The significant deviation of the data for $R < 400$ is attributed to disk vibrations. The fall off of the data for $R > 500$ is due to the highly nonlinear nature of the flow in this region and breakdown to turbulence.

Although shifting the level of the data because of uncertainty in the value of A_0 can be questioned and the resultant data cannot be used to show conclusive support for the theory, the fact that the slope of the experimental curve ($\sigma = dN/dR$) matches the present theory in the range $400 < R < 500$ is very encouraging. With recent advances in rotating equipment technology, it may be feasible to build a disk drive system with low enough vibration amplitudes in the frequency range of interest to allow an experimental estimate of A_0 to be made. Work investigating this possibility is now underway.

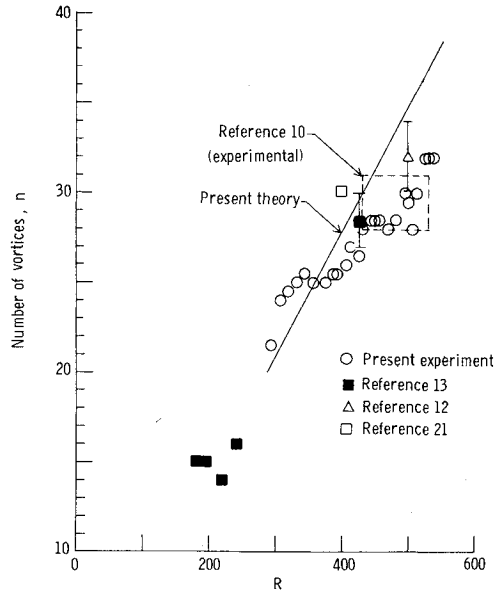

Fig. 8 Number of stationary vortices as a function of R.

Orientation and Number of Vortices

In the envelope method, we maximize growth rates $\mathrm{Im}(\omega)$ for stationary vortices over all possible wave angles. We find that the vortex spirals make an angle of about 11.2 deg with the negative of the direction of disk rotation. This is within the range of the experimental value of 11-14 deg.[10-13] The predicted angle varies very slowly with R.

It can be shown that the number of vortices is given by

$$n = \beta R \tag{33}$$

where β is defined in Eq. (15). Our calculations show that β remains almost constant ($\simeq 0.0698$) so that n varies nearly linearly with R. The numerically predicted variation of number of stationary vortices is plotted in Fig. 8 along with the experimental data. Our experimental results show that there are about 21 vortices at a Reynolds number of 294. The number of vortices increases radially and there appear about 29-31 vortices at $R \simeq 513$. This radial increase in n is apparently due to the branching of individual vortices with increasing R. Although our data fall well below the theoretical curve at high Reynolds numbers, it does substantiate the overall trend predicted by the theory.

Previous investigators[10,12,13,21] have not suggested any direct correlation between the number of vortices and the Reynolds numbers. A careful analysis of their data (Fig. 8), however, shows that their results do not necessarily disagree with the present findings. (Only a range of n and R was provided in Ref. 10.)

Parallel or Type II Instability

Lilly[15] presented numerical solutions of the Ekman layer problem and included the effect of Coriolis forces in his analysis. He found that at very low Reynolds numbers an instability mechanism exists whose disturbances are different from the stationary disturbances described previously. Lilly called this "parallel instability" and suggested that it is of a viscous type since it vanishes at high Reynolds numbers. He found that the critical Reynolds number for these fast-moving disturbances is 55, and the resulting modes are oriented at small negative angles. The orientation angle at the critical point is -23 deg, which decreases in magnitude as the Reynolds number increases. A similar instability mechanism was detected in the experiments of Faller and Kaylor[16] (who called it a type II instability) and Tatro and Mollo-Christensen.[17]

In our calculations, we also find traveling disturbances ($f \sim 100$ Hz relative to the disk) at Reynolds numbers much lower than the critical Reynolds number for stationary disturbances. The critical Reynolds number for traveling disturbances is calculated to be about 49. These disturbances appear to have characteristics similar to those reported by Lilly.[15]

VII. Conclusions

The growth of instabilities in the three-dimensional flow due to a rotating disk is studied both theoretically and experimentally. The experiments clearly show a region of linear growth that is in good agreement with linear stability theory when the effects of Coriolis forces and streamline curvature are included. Using the e^N analysis for transition prediction in these three-dimensional boundary layers, the N value is the order 11. The experiments tend to support the theoretical prediction that the number of stationary vortices increases with R.

Acknowledgments

We would like to thank W. Pfenninger for suggesting this study and D. M. Bushnell for helpful discussions. This work was sponsored by the National Aeronautics and Space Administration under Contract NAS1-15604 (MRM) and NAS1-15894 (SAO).

References

[1] Srokowski, A. J. and Orszag, S. A., "Mass Flow Requirements for LFC Wing Design," AIAA Paper 77-1222, Aug. 1977.

[2] Nayfeh, A. H., "Stability of Three-Dimensional Boundary Layers," *AIAA Journal,* Vol. 18, April 1980, pp. 406-416.

[3] Cebeci, T. and Stewartson, K., "On Stability and Transition in Three-Dimensional Flows," *AIAA Journal,* Vol. 18, April 1980, pp. 398-405.

[4] Smith, A. M. O. and Gamberoni, N., "Transition, Pressure Gradient, and Stability Theory," Douglas Aircraft Company, Rept. No. ES 26388, Aug. 1956.

[5] Hefner, J. N. and Bushnell, D. M., "Application of Stability Theory to Laminar Flow Control," AIAA Paper 79-1493, July 1979.

[6] Malik, M. R. and Orszag, S. A., "Comparison of Methods for Transition Prediction Using Three Dimensional Stability Theory," *AIAA Journal,* Vol. 18, Dec. 1980, pp. 1485-1489.

[7] Poll, D. I. A., "Some Aspects of the Flow Near a Swept Attachment Line with Particular Reference to Boundary Layer Transition," Cranfield Institute of Technology, Cranfield, C of A Rept. 7805, Aug. 1978.

[8] von Kármán, T., "Uber laminare und turbulente Reibung," *Zeitschrift für angewandte Mathematik und Mechanik,* Vol. 20, 1940, pp. 241-253.

[9] Smith, N. H., "Exploratory Investigation of Laminar Boundary Layer Oscillations on a Rotating Disk," NACA Tech. Note No. 1227, Dec. 1946.

[10] Gregory, N., Stuart, J. T., and Walker, W. S., "On the Stability of Three-Dimensional Boundary Layers with Application to the Flow Due to a Rotating Disk," *Philosophical Transactions of the Royal Society, London, Series A,* Vol. 248, 1955, pp. 155-199.

[11] Clarkson, M. H., Chin, S. C., and Shacter, P., "Flow Visualization of Inflexional Instabilities on a Rotating Disk," AIAA Paper 80-0279, Jan. 1980.

[12] Kobayashi, R., Kohama, Y., and Takamadate, Ch., "Spiral Vortices in Boundary Layer Transition Regime on a Rotating Disk," *Acta Mechanica,* Vol. 35, 1980, pp. 71-82.

[13] Fedorov, B. I., Plavnik, G. Z., Prokhorov, I. V., and Zhukhovitskii, L. G., "Transitional Flow Conditions on a Rotating Disk," *Journal of Engineering Physics,* Vol. 31, Dec. 1976, pp. 1448-1453.

[14] Brown, W. E., "Numerical Calculation of the Stability of Cross Flow Profiles in Laminar Boundary Layers on a Rotating Disk and on a Swept-Back Wing and an Exact Calculation of the Stability of the Blasius Velocity Profile," Northrop Aircraft Rept. NAI-59-5, Jan. 1959.

[15] Lilly, D. K., "On the Instability of Ekman Boundary Flow," *Journal of Atmospheric Sciences,* Vol. 23, Sept. 1966, pp. 481-494.

[16] Faller, A. J. and Kaylor, R. E., "Investigations of Stability and Transition in Rotating Boundary Layers," Edited by S. I. Pai, *Dynamics of Fluids and Plasmas,* Academic Press, New York, 1966, pp. 309-329.

[17] Tatro, P. R. and Mollo-Christensen, E. L., "Experiments on Ekman Layer Instability," *Journal of Fluid Mechanics,* Vol. 28, 1967, pp. 531-543.

[18] Orszag, S. A., "Accurate Solution of the Orr-Sommerfeld Stability Equation," *Journal of Fluid Mechanics,* Vol. 50, 1971, pp. 689-703.

[19] Gottlieb, D. and Orszag, S. A., "Numerical Analysis of Spectral Methods," NSF-CBMS Monograph No. 26, Society of Industrial and Applied Mathematics, Philadelphia, Pa., 1977.

[20] Wilkinson, J. H., *The Algebraic Eigenvalue Problem,* Oxford, 1965.

[21] Kitamura, O., "Experimental Investigation on Transition of the Boundary Layer Formed on a Rotating Disk (in Japanese)," M. S. Thesis, Dept. Mech. Eng., Hokkaido University, 1973.

[22] Gregory, N. and Walker, W. S., "Experiments on the Effect of Suction on the Flow Due to a Rotating Disk," *Journal of Fluid Mechanics,* Vol. 9, 1960, pp. 225-234.

[23] Chin, D. and Litt, M., "An Electrochemical Study of Flow Instability on a Rotating Disk," *Journal of Fluid Mechanics,* Vol. 54, 1972, pp. 613-625.

[24] Cobb, E. C. and Saunders, O. A., "Heat Transfer from a Rotating Disk," *Proceedings of the Royal Society, Series A,* Vol. 236, 1956, pp. 343-351.

[25] Bushnell, D. M., private communication, NASA Langley Research Center, June 1980.